Dynamics of the Li + Li_2 Reaction: Coexistence of Statistical and Direct Attributes

A. A. C. C. Pais, A. I. Voronin, and A. J. C. Varandas*

Departamento de Química, Universidade de Coimbra, P-3049 Coimbra Codex, Portugal

Received: October 18, 1995; In Final Form: January 3, 1996[⊗]

By using the accurate DMBE III potential energy surface for Li_3, we have carried out a detailed dynamics study of the title reaction. Besides reporting on the effect of translational and vibrational excitation of the reactants, a comparison is also presented for two models for defining the collision complex. The results support the coexistence of two different types of reaction mechanisms. One, characterized by long-lived trajectories, dominates at low-energy regimes and vibrational excitation. The other, mostly associated with direct type trajectories, starts to play a more important role at still reasonably low collisional energies, depending on the vibrational state of the reactants. It is also shown that, for initial vibrational excitation of diatomic, short-lived collision complexes can be associated with extensive randomization of vibrational energy.

1. Introduction

The exchange reactions of alkali atoms with alkali molecules M′ + $M_2(v,j)$ (M, M′ = Li, Na, K, Rb, Cs) have been the subject of many studies in the past few decades, both experimental and theoretical.[1−8] The motivation for such interest is connected with the fact that they are among the simplest exchange reactions and occur on a barrierless potential energy surface. Also interesting is the existence of important long-range dispersion forces for these systems, which can have a major effect on the reaction dynamics. In fact, the experimental measurements of reactive cross sections for the endoergic and isoergic reactions of atoms Na and K with molecules K_2, Rb_2, and Cs_2 have shown large values ($\sigma^r \geq 100$ Å^2), which are consistent with the importance of the long-range part of the involved potential energy surfaces. Furthermore, alkali trimers are convenient systems for experimental studies due to the possibility of vibrational excitation in the visible and near-infrared regions, for which good tunable lasers are available.

Alkali metal trimers are systems for which *ab initio* electronic structure calculations have been carried out.[9−17] Moreover, realistic potential energy surfaces[6,18,19] have been obtained for some of them, which can be used for dynamics studies by either quasiclassical or quantum mechanical methods. The most recent[6,19] semiempirical potential energy surfaces obtained for Li_3 are based on the double many-body expansion[20−22] (DMBE) method and take into account the normalization of the kinetic field.[23] They represent duly scaled *ab initio* data and will be used in the present work to investigate the dynamics of the Li + $Li_2(v,j)$ reaction. We also note that there have been several quasiclassical studies of the exchange reaction dynamics for the alkali metal trimers.[3,24] However, previous calculations have employed LEPS[1,2] and extended LEPS[18,25,26] forms (these include two-body dispersion forces), which cannot provide such an accurate description of both short- and long-range forces. This motivated us to investigate further the Li+$Li_2(v,j)$ exchange reaction by using the quasiclassical trajectory approach and the latest $Li_3(^2A')$ DMBE potential energy surface.[19] This study will be based on the premise that only the lowest sheet is necessary. Thus, a major goal will be to analyze the effect of translational and vibrational energy on the statistical *vs* direct nature of the title reaction. Our studies will cover a wide range of translational energies ($1 \leq E_{tr}$/kcal mol$^{-1} \leq 13.11$) and vibrational quantum numbers ($0 \leq v \leq 20$); the rotational quantum number has in all cases been fixed at $j = 10$. Attention will be given to the dependence on the translational and vibrational energies of several reaction characteristics, namely, capture and total reactive cross sections, complex lifetimes, and vibrational and angular distributions of the reaction products. Moreover, we investigate two different criteria for defining the collision complex. In one of these, the complex is viewed solely on energetic grounds, while in the other it is defined from dynamical considerations.

The plan of the paper is as follows. In section 2 we briefly discuss the main features of the DMBE potential energy surfaces for Li_3. Section 3 describes the computational procedure used in the dynamics calculations and presents our results on the influence of translational and vibrational energies in the capture and total reactive cross sections. In turn, section 4 contains an analysis of the complex lifetime distributions in terms of energetic and dynamical criteria. Section 5 describes the statistical and dynamical features of vibrational and angular distributions of products for the title reaction. The major conclusions are in section 6.

2. Potential Energy Surfaces

An important requirement for a correct description of the dynamics of chemical reactions (either quantal or quasiclassically) is to have an accurate analytical representation of the potential energy surface. The DMBE method combined with a virial decomposition analysis has been shown to attain high accuracy over all regions of interatomic distances covered in reaction dynamics. This is especially significant for the title reaction due to the important long-range forces involved in alkali atom interactions. The DMBE IA and DMBE III potential energy surfaces (described respectively in refs 6 and 19) therefore can provide a reliable description of both the fragmentation and atom−diatom channels. We note that the diatomic fragments used in these surfaces are described by the EHFACE2U[27] (extended Hartree−Fock approximate correlation energy; the digit 2 stands for diatomics and U stands for united atom limit) model, which also takes into account the normalization of the kinetic field. We further note that both DMBE functions used in this work predict the same Li_3 atomization energy, which lies within the error limits of the experimental data.[28]

Figure 1 shows a bond stretching contour plot of DMBE IA and III potential energy surfaces. Clearly, they both show the

[⊗] Abstract published in *Advance ACS Abstracts,* April 1, 1996.

S0022-3654(95)03081-4 CCC: $12.00

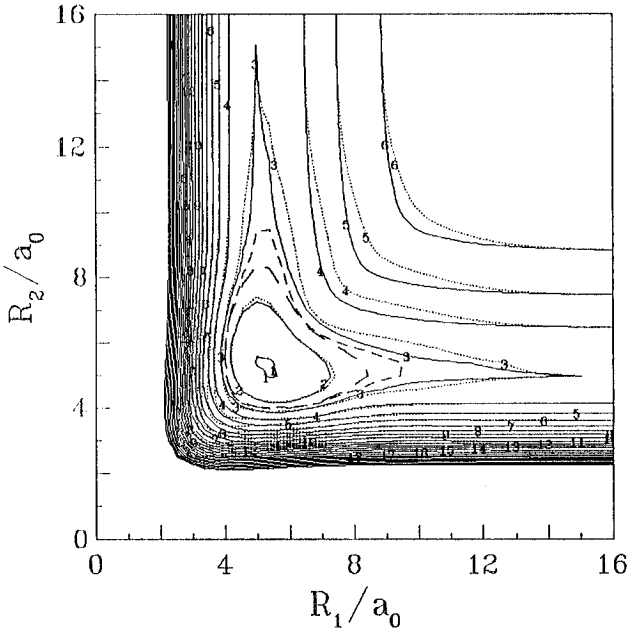

Figure 1. Stretching diagram for DMBE IA and DMBE III functions, keeping the included angle fixed at its equilibrium value ($\alpha = 70°$). Solid contours correspond to DMBE III and dotted contours to DMBE IA. Contours start at -59 mE_h relative to the separated atoms, and increase by 10 mE_h. The short-dashed and long-dashed contours encompass the regions with energy below the atom + diatom asymptote by an amount at least 20% of the Li_3 equilibrium well depth for DMBE IA and DMBE III, respectively.

same overall topographical features. It is also seen that the bond length and well depth of the $C_{2v}(^2B_2)$ equilibrium geometry are identical, while the geometries, energies, and characteristic frequencies of the most important critical points are only slightly different.[19] However, and this can also be observed in Figure 1, as one moves away from the equilibrium geometry along the minimum energy path, the lowest energy contours spread further in DMBE IA, thus revealing its more attractive nature; for further details, see ref 19.

3. Trajectory Calculations

Trajectories have been run by means of the standard quasiclassical[29−31] method. Since Li_3 is a very floppy system, corrections for zero-point energy leakage (ref 32 and references therein) were deemed unnecessary. The calculations have been carried out for collisional energies of 1, 2, 3, 6.56, and 13.11 kcal mol^{-1} and vibrational quantum numbers of the reactant diatomic of $v = 0$, 10, and 20. The rotational quantum number in all cases has been fixed at $j = 10$; the corresponding initial vibrorotational energies are 0.716, 9.987, and 17.461 kcal mol^{-1}. The collisional energies $E_{tr} = 6.56$ and 13.11 kcal mol^{-1} correspond to half of the well depth in the triatomic and to the full well depth, respectively. The first of these values is similar to that used in Na + Li_2 and Na + Na_2 molecular beam experiments (properly scaled for the difference in masses of the colliding partners). Also, the range of vibrational quantum numbers covers values found in molecular beam experiments.[33] The rotational quantum number $j = 10$ approximately corresponds to the most likely value in supersonic molecular beams,[34] while being close to that ($j = 15$) of Li_2 used in state-selected measurements.[5] Results for $j = 0$ can be found in ref 6. The value of the maximum impact parameter has been optimized in such a way that the last bin for each batch of trajectories (from $19b_{max}/20$ to b_{max}) presented no reactive trajectories.

Batches of 10^3 trajectories have been run for each specific set (E_{tr}, v, j) of initial conditions in the case of DMBE III. All trajectories have been initiated at a center of mass separation of $30a_0$, while the Li mass has been taken as that of the isotope ^{7}Li. The number of trajectories was judged satisfactory for our purposes, although for some initial conditions the actual number has been somewhat reduced. Trajectories that either did not preserve the total energy up to four decimal figures or typically exceeded 4×10^4 steps of 0.5 fs have not been included in the final statistical analysis. Although a higher degree of accuracy could have been imposed by shortening the integration time step, this would have considerably increased the computational time especially for the trajectories at low collisional energies. However, the rejection procedure adopted in the present work is probably justified at low collisional energies and initial vibrational states where the number of rejected trajectories is more significant, since one expects reactivity to be mostly statistical. In the case of DMBE IA, batches were limited to 500 trajectories, but care was taken to ensure that the total energy was preserved according to the preceding accuracy requirements or that the trajectories had been completed. Table 1 summarizes the initial conditions and results for DMBE III. It gives, from columns 1 to 6, the collisional energy, the initial vibrational quantum number, b_{max}, the reactive cross section (σ^r), the complex formation cross section (σ^c), and the number of rejected trajectories in each batch (details will be discussed later). Results for DMBE IA can be found elsewhere[6] and in Figure 2 of the present work.

TABLE 1: Summary of Initial Conditions and Quasiclassical Trajectory Results

E_{tr}/kcal mol^{-1}	v	b_{max}/Å	σ^r/Å^2	σ^c/Å^2	trajectories rejected[a]
1	0	9.1	91.9 ± 4.3	192.7 ± 4.0	179
	10	10.0	122.5 ± 4.9	211.2 ± 4.7	5
	20	11.0	160.4 ± 5.9	139.4 ± 5.8	2
2	0	8.5	60.1 ± 3.3	151.1 ± 3.5	79
	10	9.0	100.7 ± 3.9	166.0 ± 3.8	4
	20	9.6	132.3 ± 4.6	107.3 ± 4.4	2
3	0	8.0	44.8 ± 2.7	132.2 ± 3.1	30
	10	8.4	87.7 ± 3.4	143.5 ± 3.4	2
	20	9.0	116.4 ± 4.0	95.3 ± 3.9	1
6.56	0	7.2	22.5 ± 1.8	99.2 ± 2.5	10
	10	7.9	62.9 ± 2.9	105.6 ± 3.1	3
	20	8.6	87.6 ± 3.6	71.3 ± 3.4	0
13.11	0	6.1	13.8 ± 1.2	83.8 ± 1.7	3
	10	6.9	45.3 ± 2.2	84.8 ± 2.3	3
	20	7.8	49.0 ± 2.6[b]	59.3 ± 2.8	1

[a] See text. [b] There were 42 trajectories resulting in dissociation into three lithium atoms for this set of initial conditions, yielding $\sigma^{diss} = 8.0 \pm 1.2$ Å^2.

The total reactive cross sections calculated in the present work are shown as a function of translational energy in Figure 2. We observe that the dependence of $\sigma^r(E_{tr}, v)$ on E_{tr} is typical for an exoergic reaction proceeding over a barrierless potential energy surface with a chemical well. The large value of the cross section for small energies [*e.g.*, $\sigma^r(E_{tr} = 1$ kcal mol^{-1}, $v = 20) = 160.4$ Å] and its decrease with increasing energy substantiate the important role played by long-range forces. As will be seen later, such behavior is essentially controlled by capture. We also note the effect of vibrational excitation on the magnitude of the total reactive cross section. As can be seen from Figure 2, the vibrational enhancement $\sigma^r(E_{tr},v)$ at $E_{tr} = 1$ kcal mol^{-1} is $\sigma^r(v = 20)/\sigma^r(v = 0) = 1.75$. This vibrational enhancement grows considerably with energy, reaching the value 3.55 for $E_{tr} = 13.11$ kcal mol^{-1}.

At present, direct experimental measurements of the total reactive cross section and corresponding vibrational enhancement are not available for the Li + $Li_2(v,j)$ reaction. However, our results can be compared with data for the similar Na +

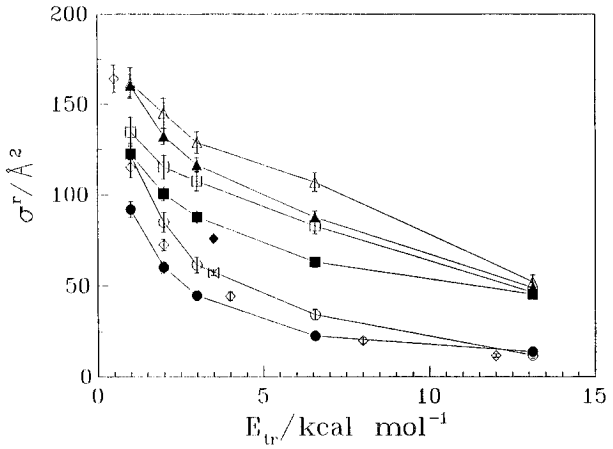

Figure 2. Reactive cross sections as a function of the collisional energy. The symbols ●, ■, and ▲ correspond to calculations based on DMBE III for $v = 0$, $v = 10$, and $v = 20$ vibrational quantum numbers of the reactant diatomic (this work), respectively. The corresponding open symbols (○, □, △) are for DMBE IA and the same vibrational quantum numbers (this work and ref 6). The symbol ◇ corresponds to values taken from ref 1. The symbols ◆ and the "bowtie" correspond to results[4] obtained by using the Varandas-Morais[25] and Thompson *et al.*[26] functions, both for $v = 0$. In all cases a rotational quantum number $j = 10$ has been used.

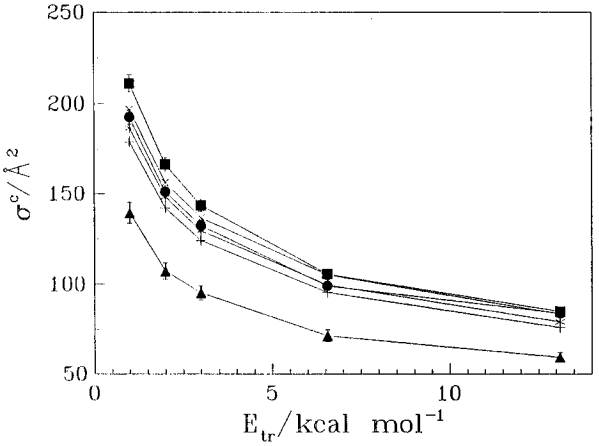

Figure 3. Complex formation cross section as a function of collisional energy. Symbols are the same as in Figure 2. Also included are the capture theory results (+, $v = 0$; *, $v = 10$; ×, $v = 20$).

$Li_2(v,j)$ reaction, which has been recently studied[7] by the molecular beam technique at $E_{tr} = 520$ meV. These experiments have suggested a total reactive cross section of less than 1 Å^2, with a vibrational enhancement in the elastic cross section of *ca.* 35%. Since a drastic dependence of the total reactive cross section on the mass of the colliding partners is unlikely to occur, and since the Li_3 potential energy surface used in the present work should be reliable, we cannot foresee a definite reason for such a disagreement. However, the Na + Li_2 reaction is slightly endoergic, and this may partly explain the observation of small reactive cross sections near the threshold energy for reaction. We also note that the use of other potential energy surfaces for the title system have only shown[1,25,26] small differences in comparison to results obtained for the DMBE IA and DMBE III potential energy surfaces. In particular, we observe that for the extreme energies (1 and 13.11 kcal mol^{-1}) considered in this work, these two last functions yield values almost indistinguishable within their error bounds except for $v = 0$. However, for the intermediate energies (especially 3 and 6.56 kcal mol^{-1}), DMBE IA shows greater reactivity as might have been anticipated from its more attractive nature. The similarity of the reactive cross section for both the lowest and highest collisional energies may then be explained as follows. For low energies, because the asymptotic part of both functions is similar, reactivity is likely to be controlled almost exclusively by capture, while for high energies the trajectories are more insensitive to the small details of the potential energy surface. The trend previously observed[6] in which reactivity increases with vibrational excitation is still present, irrespective of the potential energy surface. We also note that the discrepancy found for $v = 0$ and $E_{tr} = 1$ kcal mol^{-1} can be attributed to the relatively large number of trajectories not considered for the statistical analysis in the case of DMBE III. This fact may have somewhat biased the final result, since the statistical reactivity is nearly 2/3 (to be discussed later).

We comment next on the results obtained from previous potential energy surfaces for the title system. The most striking is the similarity between our computed reactive cross sections and those presented earlier[1] using a simple LEPS form (for the lowest relative translational energies, results for this function are placed roughly midway between DMBE I and DMBE III). We note that the only results available for this function correspond to $v = 0$, so that we are not able to assess the extension of the coincidence for other initial conditions. A more recent extended LEPS form[25] has shown[4] the highest reactivity for $v = 0$ and a collisional energy of 4 kcal mol^{-1}. Such a high reactivity is probably due to the fact that this potential energy surface has a well deeper than any of the others discussed in the present work. In what concerns the potential energy surface of Thompson *et al.*[26] calculations[4] indicate that for initial conditions restricted to $v = 0$ ($j = 10$) and a collision energy of 4 kcal mol^{-1} the reactive cross sections are similar to those interpolated from the DMBE IA results. This is not surprising since the diatomic potential curves are rather similar, and the three-body energy terms reproduce in the valence region the same[13,14] *ab initio* energies. In fact, such arguments could also be employed for the DMBE III potential energy surface, although it is clear that the differences are more substantial in this case. Note that these considerations do not necessarily apply to the case of vibrational excitation in the reactant diatomic.

We now consider the cross sections for complex formation. For collisions occurring on a potential energy surface with a potential well, the reaction is usually rationalized in terms of a two-step mechanism, in which a triatomic complex is formed before it decays to products. To calculate the cross sections for complex formation, lifetime distributions, or average complex lifetimes, one must first state the criterion from which the complex is defined. In what follows, and unless mentioned otherwise, we consider as having formed a complex[35,36] every trajectory in which the potential energy has dropped below the asymptotic atom + diatom limit by an amount equivalent to 20% of the equilibrium C_{2v} well depth; a similar criterion has been used in previous work on the O + OH reaction.[36] This can be done in a simple way by monitoring the potential energy along each trajectory, Figure 3 displays the results of calculated cross sections for complex formation. By using a simple capture model of the form (*e.g.*, ref 37)

$$\sigma(E_{tr}) = n\pi(n-2)^{(2-n)/n}\left[\frac{C_n^{Li-Li_2}(v)}{E_{tr}}\right]^{2/n} \qquad (1)$$

and by considering only the leading isotropic C_6 dispersion energy coefficient, it is possible to predict within 13% the complex formation cross sections for the two lowest vibrational quantum numbers. It is also possible to predict from eq 1 the ratios $\sigma(v = 10)/\sigma(v = 0)$ for each collisional energy, yielding

TABLE 2: Percentage of Increase in Cross Section for Complex Formation from $v = 0$ to $v = 10$[a]

E_{tr}/kcal mol^{-1}	$\sigma_c(v = 10)/\sigma_c(v = 0)$
1	9.6 (3.4)
2	9.9 (5.7)
3	8.5 (6.8)
6.56	6.5 (6.4)
13.11	1.2 (1.2)

[a] The numbers in parentheses represent values with inclusion of rejected trajectories.

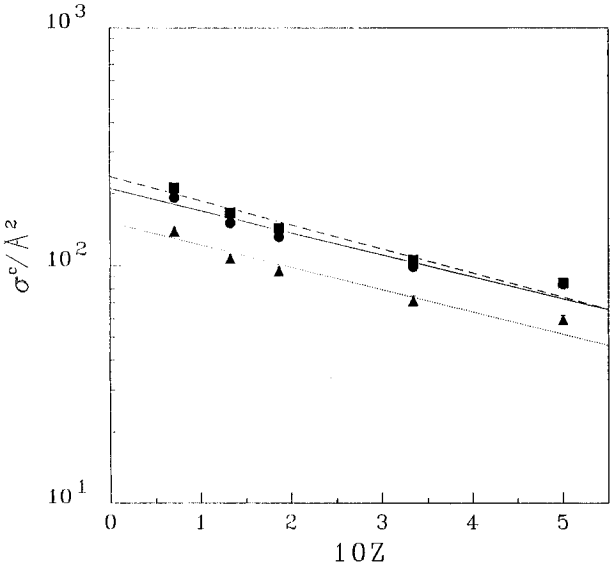

Figure 4. Complex formation cross section as a function of the RRKM parameter Z (see text). Symbols are the same as in Figure 2. The results of the fitting to eq 2 are as follows: $a_0 = 210.0$, $b_0 = 2.12$ (—); $a_{10} = 235.7$, $b_{10} = 2.32$ (— —); $a_{20} = 151.8$, $b_{20} = 2.16$ (- - -).

an increase of *ca*. 4.3% in the cross section from $v = 0$ to $v = 10$. This value does not agree with that obtained from quasiclassical trajectories (see Table 2), except when the rejected trajectories are included in the cross section for complex formation; in such a case, the agreement with the calculated values is fair. We recall that the rejected trajectories either exceeded the maximum allowed number of steps or did not preserve total energy, in any case being associated with long-lived complexes. For the highly excited reactant diatomic, the results appear to be inconsistent with a simple capture theory. This could have been anticipated from the corresponding lifetimes, as will be discussed in the following.

As shown in Figure 3, the relative magnitude of calculated complex formation cross sections $\sigma^c(v = 10) > \sigma^c(v = 0) > \sigma^c(v = 20)$ is also different from the predictions of capture theory. In this case, the relative magnitude could be rationalized by taking into account the increase in the average $C_6(v)$ dispersion coefficient with increasing vibrational excitation of the reactant diatomic, *i.e.*, $C_6(v = 20) > C_6(v = 10) > C_6(v = 0)$. However, we note that, for the highly excited $Li_2(v = 20)$ diatomic, there are a number of reactive long-distance collisions that do not lead to complex formation according to our criterion. Finally, we note from Figure 4 that a good fit of the dependence of complex formation cross section on translational energy can be obtained by using the simple exponential form

$$\sigma(E_{tr},v,j) = a_v \exp(-b_v Z) \qquad (2)$$

where a_v and b_v are constants, Z is an RRKM variable[38,39] [$Z = E_{tr}/(D + E_{tr})$], and $D = 13.11$ kcal mol^{-1} is the dissociation energy of the Li_3 complex.

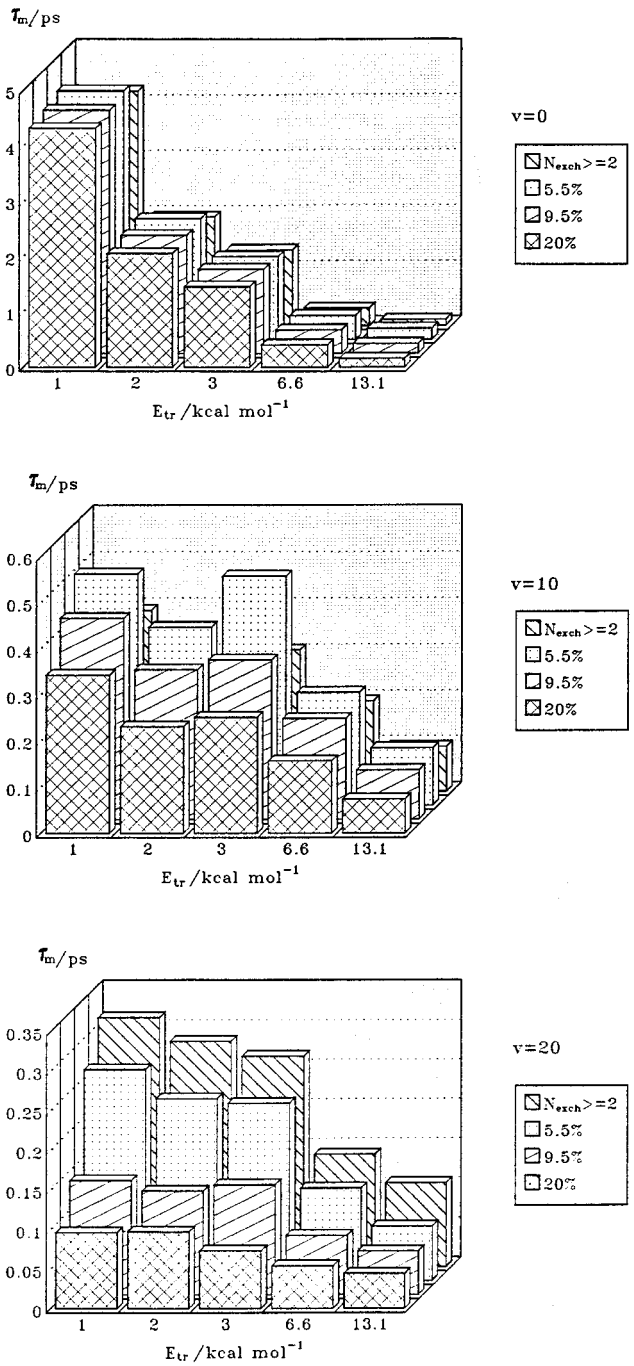

Figure 5. Average complex lifetimes as predicted from the several criteria discussed in the text.

4. Lifetimes of Li_3 Collision Complexes

We have calculated complex lifetimes, average lifetimes, and lifetime distributions according to the preceding energy criterion for defining a complex. We have also tested other values for the percentage of well depth, as well as the minimum distance exchange criterion proposed by Schlier and co-workers.[38,39] In this criterion, one counts the number of exchanges, N_{exch}, referring to the minimum bond distance; alternative definitions[1,40] of complex have been suggested in the literature, the reader being referred to the original papers for details. The energetic criteria analyzed involve 5.5, 9.5, and 20% of the well depth, while for the minimum distance exchange criterion we have considered $N_{exch} = 2$. The minimum number of exchanges $N_{exch} = 2$ has been selected because it is the least restrictive one yielding finite lifetimes (note that a trajectory that meets any of the preceding energy criteria is characterized by a

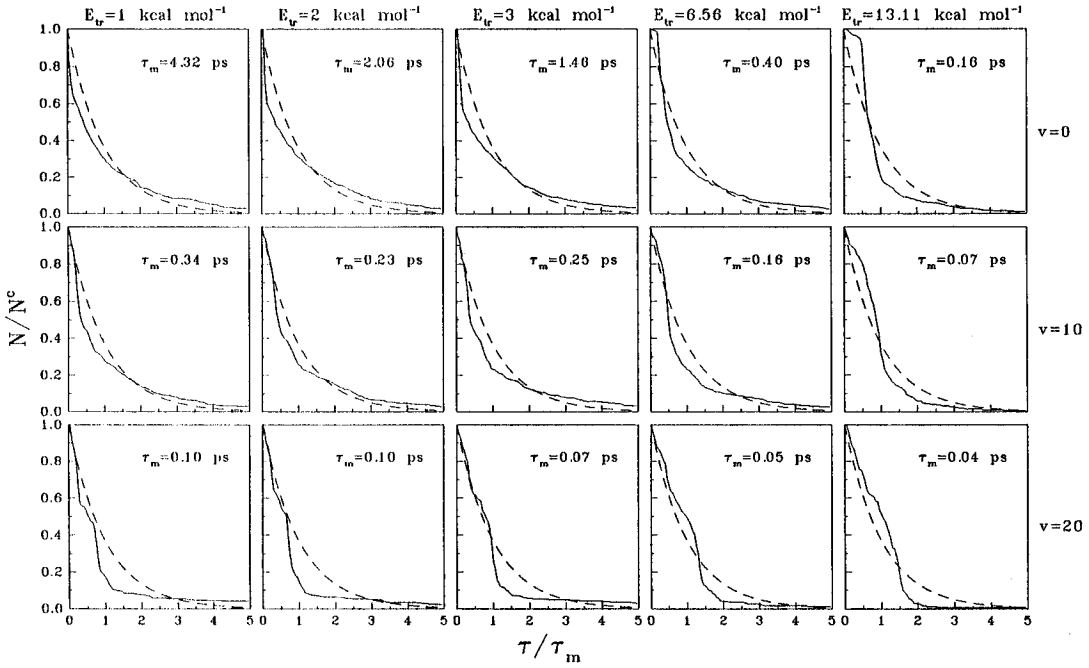

Figure 6. Fraction of complexes present at time τ (survival fraction) as a function of the reduced variable τ/τ_m, where τ_m is the average lifetime. Also indicated are the average lifetimes for each set of initial conditions. The dashed line represents $\exp(-\tau/\tau_m)$.

complex lifetime greater than zero). Other values of N_{exch} will also be discussed.

The preceding criteria have first been analyzed on the basis of the resulting average lifetime for each batch of trajectories; see Figure 5. It is seen that for $v = 0$ all criteria gave similar results, even the least restrictive one corresponding to only 5.5% of the triatomic well depth. For $v = 10$, this criterion gives the largest lifetimes. In turn, the $N_{exch} \geq 2$ criterion yields values larger than those obtained from the most restrictive energy criterion in which the trajectory must drop to potential energies below 20% of the triatomic well depth. For $v = 20$, the $N_{exch} \geq 2$ criterion predicts the longest lifetimes. This contrasts with the energy criterion of the present work, in which a sigificant part of the trajectories can be described as being of direct type. If we take into consideration that, in geometrical terms, the least restrictive energy criterion could correspond to a very "loose" complex (which includes the possibility of reactive trajectories at large distances between reactants), the collision lifetimes are probably overestimated in both this and especially the $N_{exch} \geq 2$ criterion. In fact, Schlier and co-workers[39] originally proposed $N_{exch} \geq 8$, but the increase in the number of imposed exchanges drastically reduces the number of complexes counted. Thus, this criterion is of little use for determining collision lifetimes of short-lived complexes formed from highly vibrationally excited reactants (for these, the average number of exchanges is typically between 2 and 4). Nevertheless it will be used in what follows to compare the results obtained at low collisional energies without vibrational excitation.

We now discuss the distribution of collision lifetimes (presented as the fraction of existing complexes for instant τ) shown in Figure 6. Clearly, we may identify two types of behavior: one corresponding to translational energies up to and including 6.56 kcal mol^{-1} and $v = 0$, 10 (and, probably, also with $v = 20$ and $E_{tr} = 1$ kcal mol^{-1}), and the other for high translational energies and/or vibrational quantum numbers. The latter may also be characterized by short average complex lifetimes. Figure 6 also displays the corresponding random distributions as given by

$$N/N^c = \exp(-\tau/\tau_m) \tag{3}$$

where N/N^c denotes the fraction of complexes present at instant τ, and τ_m has been determined from the quasiclassical trajectory results. We see that this distribution is roughly followed for lower collisional energies and low vibrational excitation of the reactant diatomic. As the average lifetime decreases, deviations from this simple behavior become progressively more noticeable.

It may now prove useful to compare the average lifetimes τ_m presented in Figure 6 with the rotational period of the Li_3 collisional complex $\tau_r = 2\pi(I/L) = 0.4$ ps (I is the moment of inertia of the complex and L is its orbital angular momentum) and the vibrational periods for the three fundamental frequencies of the Li_3 molecule $\tau_v = 0.569$, 1.011, and 1.386 ps. We observe that the average lifetime for the second type of distribution is significantly less than the rotational and vibrational periods, and, therefore the collision complexes do not comply with their traditional definition. Having that in mind, we can say that only those of the first type describe the nearly statistical nature of the Li + Li_2 collision dynamics for the corresponding energies and vibrational quantum numbers. The second type essentially corresponds to direct type trajectories.

Figure 7 shows the average complex lifetimes as a function of the translational energy for each vibrational quantum number. Usually, the functional form used to fit this dependence corresponds to some power law[38]

$$\tau_m = \tau_0 Z^{-s} \tag{4}$$

where Z has the meaning previously assigned. We have found, however, that a more adequate representation would be the simple exponential form

$$\tau_m = \tau_0 \exp(-\gamma Z) \tag{5}$$

where τ_0 and γ are adjustable parameters. The least-squares fits are shown by the solid lines in Figure 7. The quality of the final result implies that the average complex lifetimes are not so sensitive to the statistical nature of the complex as the lifetime distributions themselves. It should be noted that eq 4 is sometimes adequate to describe unimolecular decomposition,

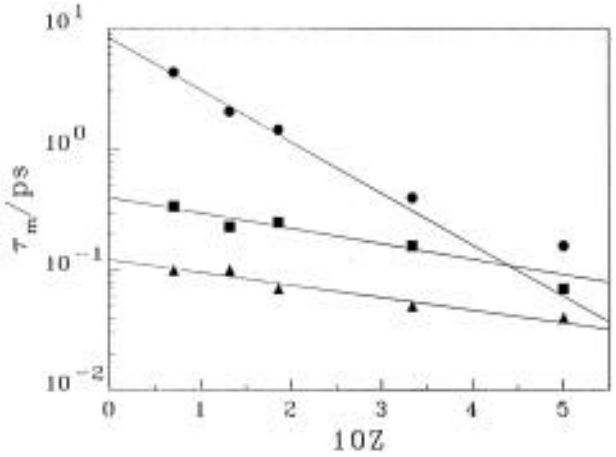

Figure 7. Average complex lifetimes as a function of Z. Symbols are the same as in Figure 2. The parameters τ_0, γ take the values (8.35, 9.85), (0.40, 2.93), and (0.12, 2.43) for $v = 0$, $v = 10$, and $v = 20$, respectively.

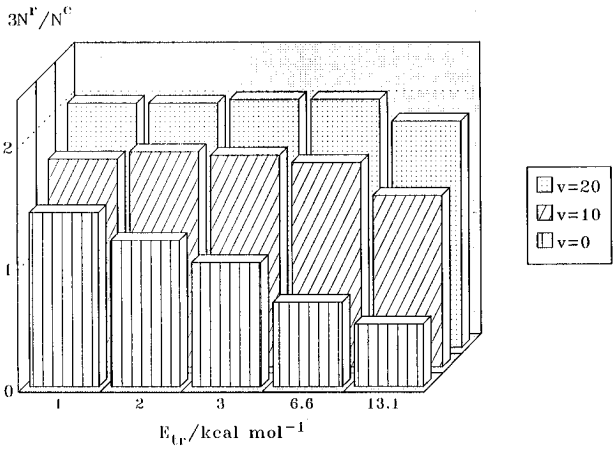

Figure 8. Ratios of the number of reactive complexes, entering complex region, to the number of complex-forming trajectories.

yielding an infinite average lifetime for $Z = 0$. Thus, it does not generally apply to complexes formed in bimolecular collisions occurring on a potential energy surface with a well. Because there is always a nonvanishing translational energy when entering or leaving the complex region, as defined in the present work, the average complex lifetimes must remain finite as Z approaches zero.

Let us now investigate the effect of average lifetime on the subset of complex trajectories that are reactive. Figure 8 displays the translational energy dependence of the fraction of reactive complexes, N^r/N^c. For $v = 10$, we observe that these fractions have a small dependence on the collisional energy and are placed slightly below 2/3. For $v = 20$, they are almost energy independent and consistently close to 2/3. For the lowest reactant diatomic vibrational quantum numbers, the ratio decreases markedly with increasing translational energy, starting slightly above 1/3. All of these results correspond to our 20% energy criterion. Focusing on the lowest energies and $v = 0$ (Figure 9), we see that a reduction in the number of complexes by imposing a threshold of successively longer lifetimes has two effects: the ratios become more independent of energy and tend to approach 2/3. The same results would naturally be obtained if N_{exch} was increased in the minimum number of exchanges criterion; see Figure 9b. The limit of 2/3 for the ratio of reactive trajectories to those forming a complex may simply be explained[37] by the availability of three equivalent channels (one nonreactive and two reactive) on the Li_3 potential energy surface.

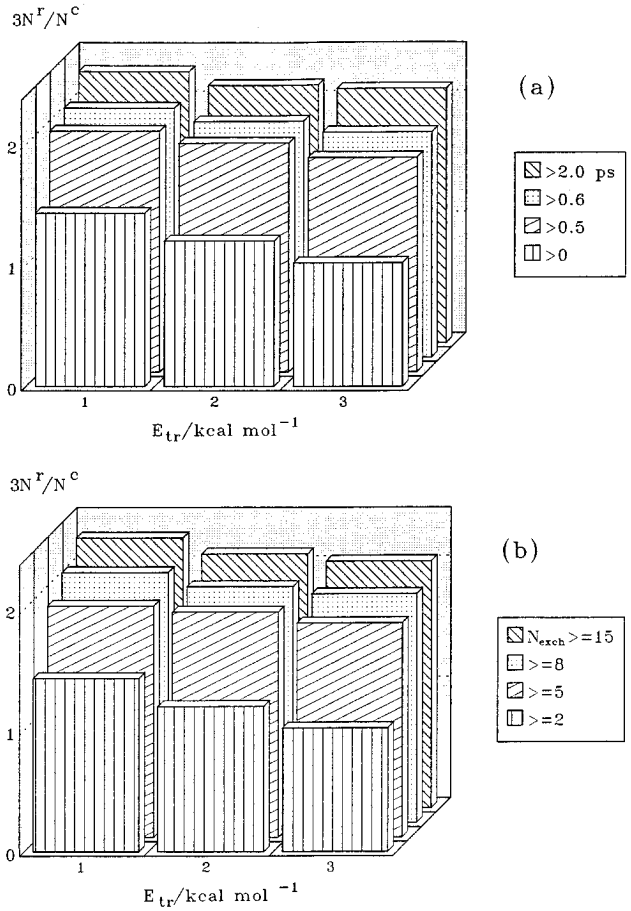

Figure 9. Same as Figure 8 for $v = 0$ and different imposed thresholds of (a) lifetime and (b) N_{exch} for the 20% well depth energy and number of minimum exchanges criterion, respectively.

5. Vibrational and Angular Distributions

Let us now briefly discuss the angular and vibrational distributions of the products for the title exchange reaction. As follows from the preceding comparison of the rotational period and average lifetime, the average complex lifetimes found with values similar to or greater than that of the predicted rotational period include $v = 0$ and $E_{tr} = 1$, 2, and 3 kcal mol^{-1}. Figure 10 shows that these three cases seem to favor backward scattering, and the same behavior is present, irrespective of relative translational energy, for $v = 0$. The increase in vibrational quantum number, especially for high energies, clearly points to forward scattering. In spite of the uncertainty associated with angles near 0° and 180°, the general behavior is that peak intensity for forward scattering increases with decreasing average complex lifetime, as could be expected from the osculating complex model.

The vibrational distribution of products is shown in Figure 11 and reveals two types of behavior. For $v = 0$, we find a thermal distribution, with the population of excited states increasing with translational energy. For the other two reactant vibrational quantum numbers, the distributions are either almost uniform or peak at some intermediate value of v' before decaying rapidly for higher excited states. The latter type of behavior is similar to that previously observed in trajectory calculations, namely, for the Cl + $Cl_2(v)$ reaction.[41,42] Although nonthermal product vibrational distributions (which occur in the present work for highly vibrationally excited reactants or high collisional energies) are often attributed to incomplete energy randomization, this picture is somewhat contradicted by the results described in the previous section, which show that

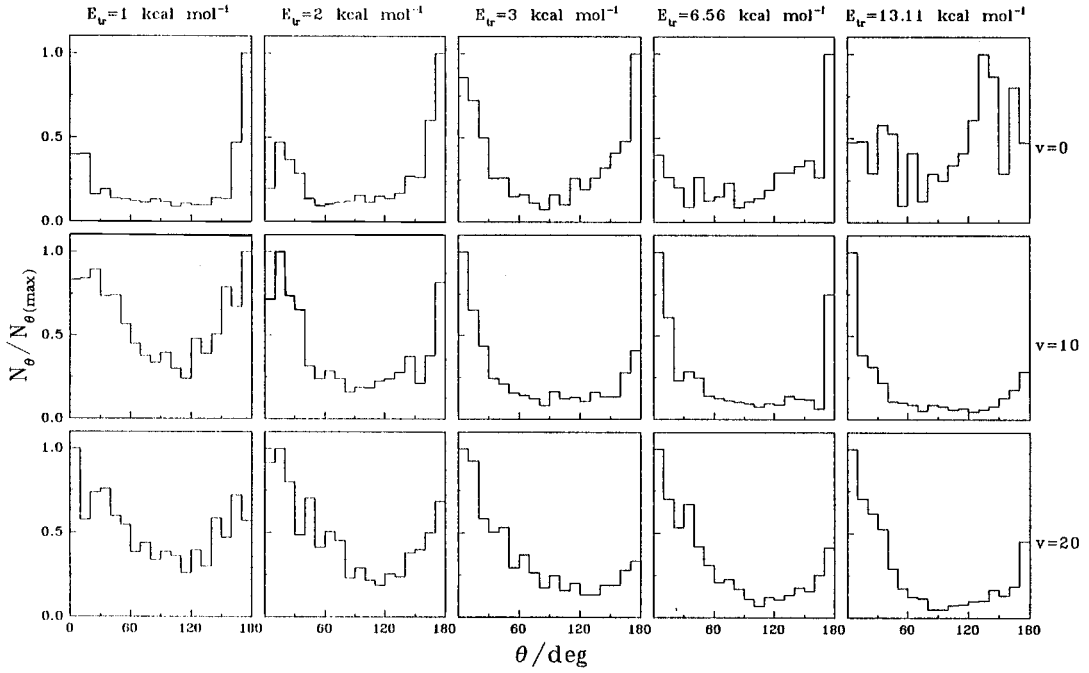

Figure 10. Scattering angle distribution for reactive trajectories. Results are presented for each set of initial conditions.

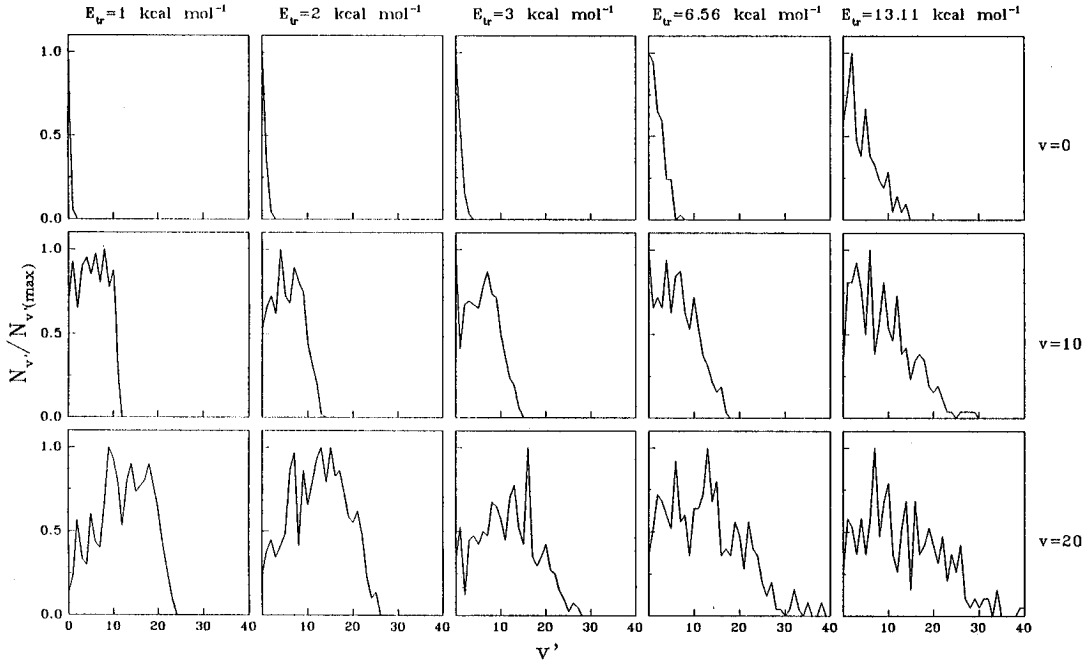

Figure 11. Vibrational distribution in reactive trajectories for each set of initial conditions.

vibrational excitation of the reactants leads to equal accessibility of all channels.

Figure 12 presents the average internal energy of the product diatomic for each set of initial conditions as a function of the collision energy. The general behavior is consistent with the hybrid statistical/stripping-spectator[8] model recently proposed, especially for the initial vibrational quantum numbers $v = 0$ and $v = 10$. Indeed, the final internal energy is shown to linearly depend on the initial translational energy. This suggests that a constant fraction of the latter is transformed into internal energy (this fraction is very similar for $v = 0$ and $v = 10$ in the range of collisional energies considered in the present work, since the corresponding lines are almost parallel), while a constant fraction of this goes to the product molecule. For $v = 20$, conditions appear to be too extreme to be explained through this simple model.

6. Conclusions

A detailed study of the title reaction has been presented by using an accurate potential energy surface for ground state $Li_3(^2A')$. The assumption has been made that the reaction occurs adiabatically on the lowest doublet state surface. For a variety of initial conditions, we have reported results on the influence of translational and vibrational energies on capture and total reactive cross sections and vibrational and angular distributions of products. Moreover, we have presented an analysis of the complex lifetime distributions in terms of energetic and dynamical criteria. The results support the idea of a wide range of behaviors depending on the initial conditions of the reactants. For low energies, the data suggest that a statistical mechanism prevails, while a direct mechanism is probably dominant at high translational energies and/or vibrational excitation of the reactant

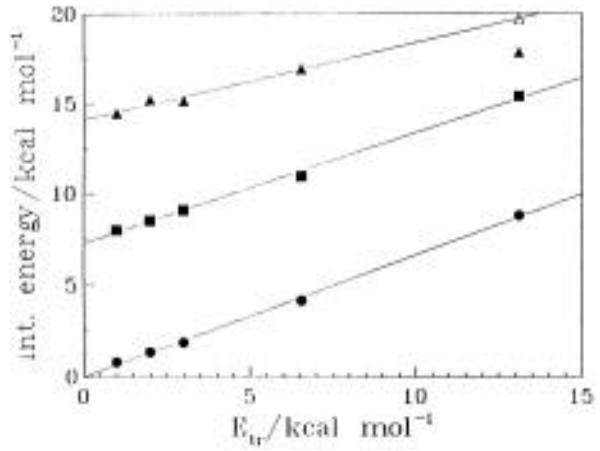

Figure 12. Internal energy of the product diatomic as a function of translational energy. Symbols are the same as in Figure 2. The point corresponding to $E_{tr} = 13.11$ kcal mol^{-1}, $v = 20$, does not include dissociative trajectories in the average energy and has not been considered in the fitting procedure. The corresponding open symbol includes dissociative trajectories with internal energy equal to the well depth of the diatomic and also has not been considered for the fitting procedure.

molecule. A comparative study has also been carried out for two models defining collision complex. These models, one based on energetic grounds and the other[38] on dynamical ones, have been shown to give similar results for low initial vibrational states of the reactants. For high vibrational states, the use of a bond-exchange[38] model may become problematic since the number of bond exchanges is always found to be $N_{exch} < 8$, while some trajectories are clearly of the long-lived type.

Acknowledgment. A.I.V. thanks the International Association for the Promotion of Cooperation with Scientists from the Independent States of the former Soviet Union and INVOTAN for financial support. This work is sponsored by Junta Nacional de Investigação Científica e Tecnológica, Portugal.

References and Notes

(1) Whitehead, J. C. *Mol. Phys.* **1975**, *29*, 177.
(2) Whitehead, J. C. *Mol. Phys.* **1976**, *31*, 549.
(3) Morais, V. M. F.; Varandas, A. J. C. *J. Chem. Soc., Faraday Trans. 2* **1987**, *83*, 2247.
(4) Morais, V. M. F.; Varandas, A. J. C. *J. Chem. Soc., Faraday Trans. 2* **1989**, *85*, 1.
(5) Rubahn, H.-G. *J. Phys. Chem.* **1991**, *95*, 8215.
(6) Varandas, A. J. C.; Pais, A. A. C. C. *J. Chem. Soc., Faraday Trans.* **1993**, *89*, 1511.
(7) Rubahn, H.-G.; Slenczka, A.; Toennies, J. P. *J. Chem. Phys.* **1994**, *101*, 1262.
(8) Morais, V. M. F.; Varandas, A. J. C. *Mol. Phys.* **1995**, *84*, 957.
(9) Yardley, R. N.; Balint-Kurti, G. G. *Chem. Phys.* **1976**, *16*, 287.
(10) Kendrick, J.; Hillier, H. *Mol. Phys.* **1977**, *33*, 635.
(11) Davies, D. W.; Del Conde, G. *Chem. Phys.* **1976**, *12*, 45.
(12) Bagus, P. S.; Del Conde, G.; Davies, D. W. *Faraday Discuss. Chem. Soc.* **1977**, *62*, 321.
(13) Gerber, W. H.; Schumacher, E. *J. Chem. Phys.* **1978**, *69*, 1692.
(14) Gerber, W. H. Ph.D. Thesis, University of Bern, 1980.
(15) Gole, J. L.; Childs, R. H.; Dixon, D. A.; Eades, R. A. *J. Chem. Phys.* **1980**, *72*, 6368.
(16) Beckmann, H.-O. *Chem. Phys. Lett.* **1982**, *93*, 240.
(17) Martins, J. L.; Car, R.; Buttet, J. *J. Chem. Phys.* **1983**, *78*, 5646.
(18) Varandas, A. J. C.; Morais, V. M. F.; Pais, A. A. C. C. *Mol. Phys.* **1986**, *58*, 285.
(19) Pais, A. A. C. C.; Nalewajski, R. F.; Varandas, A. J. C. *J. Chem. Soc., Faraday Trans.* **1994**, *90*, 1381.
(20) Varandas, A. J. C. *Adv. Chem. Phys.* **1988**, *74*, 255.
(21) Varandas, A. J. C. *Chem. Phys. Lett.* **1992**, *194*, 333.
(22) Varandas, A. J. C. *Dynamical Processes in Atomic and Molecular Physics*; Delgado-Barrio, G., Ed.; IOP Publishing: Bristol, 1993; p 3.
(23) Varandas, A. J. C.; Nalewajski, R. F. *Chem. Phys. Lett.* **1993**, *205*, 253.
(24) Whitehead, J. C.; Grice, R. *Mol. Phys.* **1973**, *26*, 267.
(25) Varandas, A. J. C.; Morais, V. M. F. *Mol. Phys.* **1982**, *47*, 1241.
(26) Thompson, T. C.; Izmirlian, G., Jr.; Lemon, S. J.; Truhlar, D. G.; Alden Mead, C. *J. Chem. Phys.* **1985**, *82*, 5597.
(27) Varandas, A. J. C.; Silva, J. D. *J. Chem. Soc., Faraday Trans.* **1992**, *88*, 941.
(28) Wu, C. H. *J. Chem. Phys.* **1976**, *65*, 3181.
(29) Karplus, M.; Porter, R. N.; Sharma, R. D. *J. Chem. Phys.* **1965**, *43*, 3259.
(30) Bunker, D. L. *Methods Comp. Phys.* **1971**, *10*, 287.
(31) Truhlar, D. G.; Muckerman, J. T. *Atom-Molecule Collision Theory*; Bernstein, R. B., Ed.; Plenum Press: New York, 1979; p 505.
(32) Varandas, A. J. C.; Marques, J. M. C. *J. Chem. Phys.* **1994**, *100*, 1908.
(33) Rubahn, H.-G.; Bergmann, K. *Annu. Rev. Phys. Chem.* **1990**, *41*, 735.
(34) Sinha, M. P.; Schultz, A.; Zare, R. N. *J. Chem. Phys.* **1973**, *58*, 549.
(35) Quintales, L. A. M.; Varandas, A. J. C.; Alvariño, J. M. *J. Phys. Chem.* **1988**, *92*, 4552.
(36) Varandas, A. J. C.; Brandão, J.; Quintales, L. A. M. *J. Phys. Chem.* **1988**, *92*, 3732.
(37) Varandas, A. J. C. *Conferencias Plenarias de la XXIII Reunión Bienal de Química*; San Feliciano, A., Grande, M., Casado, J., Eds.; R.S.E.Q.: Salamanca, 1991; p 321.
(38) Schlier, C.; Vix, U. *Chem. Phys.* **1985**, *95*, 401.
(39) Brass, O.; Schlier, C. *J. Chem. Soc., Faraday Trans.* **1993**, *89*, 1533.
(40) Bonnet, L.; Rayez, J. C.; Halvick, P. *J. Chem. Phys.* **1993**, *99*, 1771.
(41) Procaccia, I.; Levine, R. D. *J. Chem. Phys.* **1975**, *62*, 2496.
(42) Levine, R. D.; Bernstein, R. B. *Dynamics of Molecular Collisions B*; Miller, W. H., Ed.; Plenum: New York, 1976; p 323.

JP9530818